Sexual dimorphism in sensorimotor transformation of optic flow

Sarah Nicholas[1], Katja Sporar Klinge[1#], Luke Turnbull[1], Annabel Moran[1], Aika Young[1], Yuri Ogawa[1], Karin Nordström[1,2*]*

[1]Flinders Health and Medical Research Institute, Flinders University, GPO Box 2100, Adelaide, SA, 5001, Australia; [2]Department of Medical Cell Biology, Uppsala University, 75123 Uppsala, Sweden.

[#]Current address: Institute for Developmental Biology, RWTH Aachen University, 52074 Aachen, Germany

*Shared authorship; email: karin.nordstrom@flinders.edu.au; yuri.ogawa@flinders.edu.au

ORCIDs

Sarah Nicholas: 0000-0002-5555-9421

Katja Sporar Klinge: 0009-0004-7224-6568

Aika Young: 0009-0000-5028-6164

Karin Nordström: 0000-0002-6020-6348

Yuri Ogawa: 0000-0002-9708-7063

CRediT author statement

Sarah Nicholas: conceptualization, methodology, validation, formal analysis, investigation, data curation, writing – original draft, visualization; **Katja Sporar Klinge:** methodology,

validation, formal analysis, investigation, data curation, writing – review and editing, visualization; **Luke Turnbull:** methodology, validation, investigation, writing – review and editing; **Annabel Moran:** investigation, writing – review and editing; **Aika Young**: investigation, writing – review and editing; **Karin Nordström:** conceptualization, validation, formal analysis, resources, writing – original draft, visualization, supervision, project administration, funding acquisition; **Yuri Ogawa:** methodology, validation, formal analysis, investigation, data curation, writing – original draft, visualization, supervision, project administration.

Abstract

Motion vision underpins a wide range of adaptive behaviours essential for individual and species survival. Some visual behaviours are sexually dimorphic, including for example male hoverfly high-speed pursuit of conspecifics, matched by improved optics, and faster photoreceptors. Other visual behaviours are monomorphic, with for example similar foraging flight speeds in male and female hoverflies. However, whether the descending neurons responsible for sensorimotor transformation of optic flow are sexually dimorphic is unknown. To redress this, we combined morphological analysis with electrophysiology of optic flow sensitive descending neurons and compared neural responses to the wing beat amplitude in tethered hoverflies. We found that while optomotor flight behaviour is largely sexually monomorphic, the underlying neural responses are sexually dimorphic, especially at higher optic flow velocities. Additionally, neural and behavioural responses to roll stimuli had a slower onset compared to lift, revealing stimulus specific encoding. Together, our findings uncover a nuanced, sex- and stimulus- dependant sensorimotor transformation, shaped by both neural architecture and behavioural demands.

Keywords

Sexual dimorphism, hoverfly, descending neuron, optic flow, optomotor response

45 ## Introduction

46 Motion vision is a fundamental sensory modality across the animal kingdom, enabling
47 animals to navigate, to maintain a straight trajectory, to avoid collisions, and to identify prey,
48 predators or mates. Among the most potent cues for self-motion is optic flow, the coherent
49 motion of the entire visual field, generated by an animal's own movement through the world.
50 In insects, the neural mechanisms underlying optic flow processing have been studied
51 extensively (for a review, see e.g. Ref [1]), offering a powerful model for understanding how
52 compact nervous systems extract behaviourally relevant information from dynamic visual
53 scenes.

54 To generate appropriate responses to widefield optic flow, the visual input needs to be
55 integrated across space. In flies, this spatial pooling occurs in lobula plate tangential cells
56 (LPTCs), each matched to a particular type of self-generated optic flow[2]. For example,
57 neurons of the horizontal system (HS cells) respond optimally to rotations around the yaw
58 axis, whereas neurons in the vertical system (VS cells) are tuned to pitch and roll rotations[3].
59 While LPTCs process widefield optic flow their role in the resulting behaviours[4,5] is indirect,
60 via optic flow sensitive descending neurons that therefore play a key role in sensorimotor
61 transformation[6,7]. In *Drosophila* and blowflies, there are three main optic flow sensitive
62 descending neurons. DNHS1, also called NDp15[8], receives input from HS cells[6,7] and is
63 physiologically similar to the optic flow sensitive descending neuron type 1 (OFS DN1) in
64 the hoverfly *Eristalis tenax*[9]. DNHS1 has been implicated in the control of head yaw
65 movements and abdominal ruddering and may engage with the haltere motor system for

flight stabilization[6]. DNOVS1, or DNp20[8], receiving input from the ocelli and VS cells[6,10], is likely involved in rapid head movements, possibly facilitating gaze stabilization during flight[6]. DNOVS2, or DNp22[8], also receives input from the ocelli but a different subset of VS cells[6,11] and is physiologically similar to the *Eristalis tenax* optic flow sensitive descending neuron type 2 (OFS DN2)[9]. DNOVS2 is well suited to initiate the fast body saccades that support rapid re-orientation[6] during flight in response to dynamic visual cues.

Hoverflies are interesting in the context of motion vision, which they use both to maintain a hovering stance, and to fly at high speed[12]. Indeed, hoverflies show striking sexually dimorphic flight behaviour, where males establish territories which they guard rigorously[13] to chase away any intruding insects and/or pursue conspecific females for courtship and mating[12,14]. Accompanying this behaviour, male *E. tenax* have larger lenses than females in a dorso-frontal bright zone[15], with faster motion detection and increased signal-to-noise ratio[16]. In many fly species, the photoreceptors in this part of the eye are also faster in males[17]. In hoverflies, some LPTCs are sexually dimorphic, with males having a smaller HSN receptive field[18] and velocity tuning shifted to higher velocities[15,19]. The differences in optics, photoreceptor dynamics, and LPTC receptive field size and velocity tuning, have been interpreted as required by males in the fast flight used during sexually dimorphic territorial behaviours. Interestingly, male hoverflies are also smaller than females[20,21], which introduces an aerodynamic component to these behavioural and sensory specializations by reducing inertia and enabling finer control over rapid flight adjustments[22]. However, there is no sexual dimorphism in flight speed during non-courtship activities such as foraging between flowers[23] nor when flying within the confines of an indoor arena[24].

88 To investigate the discrepancy between sexually dimorphic visual processing and sexually
89 monomorphic behaviours, we compared the electrophysiological response characteristics and
90 morphology of optic flow sensitive descending neurons in male and female hoverflies and
91 linked these findings to the wing beat amplitude (WBA) of tethered hoverflies viewing
92 similar stimuli. The optomotor responses confirm free flight observations by showing limited
93 sexual dimorphism at speeds up to 2 m/s for translation and 200°/s for rotation. However,
94 while neural morphology, receptive fields and direction sensitivity of the descending neurons
95 showed minimal sex differences, there was a significant and noticeable difference in the
96 velocity response functions between males and females, especially at higher speeds.
97 Critically, neural differences were not only velocity dependent but also varied between
98 stimuli (occurring only for sideslip, lift and thrust, but not roll) and neuron type. Furthermore,
99 we found a striking difference in response onset between lift and roll in OFS DN2 and WBA,
100 but not OFS DN1. These neuron-, stimulus-, and sex-specific differences uncovers a
101 previously unrecognized complexity in the neural encoding of visual motion, revealing for
102 the first time, a sex-dependent transformation from sensory input to motor output.

103 Results

104 Two distinct types of optic flow sensitive descending neurons can be identified by their
105 receptive field location and preferred direction

106 Optic flow sensitive descending neurons can be readily identified by mapping their receptive
107 field using small sinusoidal gratings[9,15]. Based on the receptive fields of 100 reference
108 neurons recorded from 90 male hoverflies, we found that two key parameters, the position of

109 the receptive field centre and its preferred direction of motion, are sufficient to reliably
110 ascertain neuron type (Fig. 1). OFS DN1 has a preferred direction up and away from the
111 midline, either leftward (range from 137° to 171°) or rightward (range from 16° to 40°) for
112 neurons on the left- and right-hand side of the visual field, respectively (Fig. 1a, b and c;
113 green, Fig. 1g, h and i). OFS DN2 neurons respond preferentially to downward motion (range
114 from 228° to 293°; Fig. 1d, e and f; yellow and orange, Fig. 1g, h and i) with the position of
115 the receptive field centre relative to the midline separating left hand side (LHS) from right
116 hand side neurons (RHS, Fig. 1g, h and i).

117 We used the maximum local motion sensitivity (LMS, Fig. 1c, f), the extent of the receptive
118 fields (number of positions with LMS over 50%, Fig. 1c, d) and the local preferred direction
119 (LPD, Fig. 1c, d) variance from these 100 reference neurons (grey data, Supplementary Fig.
120 1a, b and c) to set strict exclusion criteria (dashed red, Supplementary Fig. 1a, b and c) of the
121 neurons used in the rest of the paper. This resulted in the exclusion of two neurons from
122 males and seven from females (grey, Supplementary Fig. 1d, e) due to either low LMS (less
123 than 20 spikes/s, Supplementary Fig. 1a), a small number of locations where LMS exceeded
124 50% of the maximum (4 positions or less, Supplementary Fig. 1b) or high LPD variance
125 (above 30°, Supplementary Fig. 1c). A comparison of the remaining 33 male and 29 female
126 neurons showed no significant sexual dimorphism in receptive field size for either neuron
127 type (Supplementary Fig. 1f, unpaired t-test, $p = 0.52$ and 0.09 for width and height of OFS
128 DN1, and $p = 0.19$ and 0.13 for width and height of OFS DN2).

129 **Directional tuning of optic flow sensitive descending neurons exhibits limited sexual**
130 **dimorphism**

131 Some LPTCs, which are upstream of the descending neurons, show distinct sexual
132 dimorphism, whilst others do not[15,18]. To determine the extent of sexual dimorphism in the
133 descending neurons, we compared the direction tuning of males and females in response to
134 full screen stimuli. When presented with full-screen sinusoidal gratings (wavelength 7°, 5
135 Hz), the preferred direction of both OFS DN1 and OFS DN2 matched their receptive field
136 preferred directions (Supplementary Fig. 1d, e and Supplementary Fig. 2c, d), i.e. up and
137 away from the visual midline for OFS DN1 (range from 359° to 52°) or downwards for OFS
138 DN2 (range from 273° to 297°, Fig. 2a). Whilst OFS DN1 showed no difference in preferred
139 direction between the sexes (Watson-Williams two-sample test, $p = 0.38$), male OFS DN2
140 had a slightly more lateral preferred direction compared to females (Fig. 2a; median = 285.4°
141 compared to 281.5°, Watson-Williams two-sample test, $p = 0.046$).

142 We next looked at the responses to 3-dimensional starfield stimuli simulating the type of
143 optic flow that would be generated by self-motion through space[25]. Neither the spontaneous
144 rate nor the responses of OFS DN1 to a stationary starfield pattern differed between the sexes
145 (circles, Supplementary Fig. 3a, two-way ANOVA, $p = 0.29$). Conversely, OFS DN2
146 exhibited significant sexual dimorphism, with a higher spontaneous rate and response to
147 stationary stimuli in females compared to males (circles, Supplementary Fig. 3b, two-way
148 ANOVA, $p < 0.001$). To determine if there was additional sexually dimorphic dependence on
149 the type of optic flow, we subtracted the response to the stationary stimulus from the

150 responses to each direction of the optic flow (0.5 m/s for translations and 50°/s for rotations)
151 within each trial. As predicted from the receptive fields (Fig. 1) OFS DN1 was excited by
152 stimuli moving either up or away from the midline, such as rightward sideslip and yaw, and
153 upwards lift and pitch (Fig. 2b), whilst OFS DN2 showed the strongest responses to
154 downwards lift and pitch (Fig. 2c). Both neuron types respond strongly to clockwise roll, as
155 predicted by their receptive fields (Fig. 1a, b) and shown previously for males[9]. However,
156 neither neuron type showed any sexual dimorphism (Fig. 2b, c, two-way ANOVA, $p = 0.81$
157 and 0.92, OFS DN1 and OFS DN2, respectively).

158 **Sexual dimorphism in optic flow descending neurons is velocity dependent**

159 As the velocity tuning of some LPTCs is sexually dimorphic[15,19], we tested the responses of
160 optic flow sensitive descending neurons using a continuous velocity step stimulus (Fig. 3,
161 Supplementary movie 1). Six velocities for each direction of the stimuli (e.g. anticlockwise
162 roll -10 to -200°/s and clockwise roll +10 to +200°/s) and a stationary control were presented
163 3 times each in random order for 2 s each (see example, Fig. 3a).

164 We confirmed that the spontaneous rate and response to stationary stimuli was significantly
165 higher in females compared to males for OFS DN2 but not for OFS DN1 (triangles,
166 Supplementary Fig. 3b, two-way ANOVA, $p = 0.18$ and $p < 0.001$, OFS DN1 and OFS DN2,
167 respectively). As above, we subtracted each trial's average response to the stationary stimulus
168 from the responses to moving optic flow. The resulting data show that both neuron types
169 exhibit sexual dimorphism to certain types of optic flow (Fig. 3e, f and Table 1). For

170 example, the OFS DN1 response to thrust show a significant interaction between sex and
171 velocity, with female neurons responding stronger to positive thrust compared to males (Fig.
172 3e and Table 1). The OFS DN2 response to sideslip was significantly different between males
173 and females, and there was a significant interaction between sex and velocity in the responses
174 to sideslip, lift, and thrust, with males responding stronger to sideslip, lift and thrust (Fig. 3f
175 and Table 1).

176 **Morphological reconstruction suggests optic flow sensitive neurons could control wing**
177 **movements**

178 By recording from the descending neurons intracellularly we could iontophoretically fill them
179 with 3% neurobiotin following identification based on receptive field (as in Fig. 1). We found
180 that OFS DN1 and OFS DN2 of either sex receive their input in the part of the brain where
181 LPTCs have their output (Fig. 4). Both neuron types also have wide branches projecting to
182 the area of the thoracic ganglion where the prothoracic and pterothoracic nerves likely get
183 their inputs (T1 LN and PtN, Fig. 4a), suggesting they could contribute to controlling the
184 wings and/or the forelegs. Whilst there was no indication of extensive sexual dimorphism in
185 the structural morphology of these neurons, OFS DN2 appears to be slightly wider along the
186 length of the cervical connective in females (Supplementary Fig. 4b). In part, this may be due
187 to female hoverflies being bigger[20,21] and therefore having a wider cervical connective
188 (Supplementary Fig. 4c).

189

190 **Wing beat amplitude changes are velocity dependent but not sexually dimorphic**

191 Given that the morphological data suggest that both neuron types could control the wings
192 (Fig. 4), we conducted behavioural experiments in an open-loop tethered flight arena using
193 the same continuous velocity stimulus as in electrophysiology (see Fig. 3a). We tracked the
194 wing beat amplitude (WBA) for each wing (Fig. 5a, b, Supplementary movie 2) using
195 DeepLabCut models[26,27] while the tethered animal was viewing different starfield velocities
196 (Fig. 5c-f). Changes in the sum of the left and right WBA (WBAS) reflect variations in flight
197 force generation, potentially contributing to either lift or thrust, while the difference between
198 left and right WBA (WBAD) indicates yaw turning behaviour[28-30] or adjustments to body
199 orientation[31].

200 The male WBAS is higher when viewing stationary stimuli compared with pre-stimulation
201 ("pre stim", Fig. 5c, d; two-way ANOVA followed by Uncorrected Fisher's LSD test,
202 $p < 0.0001$, blue squares, Supplementary Fig. 3c). The male WBAS was also larger than in
203 female hoverflies viewing stationary stimuli (two-way ANOVA followed by Uncorrected
204 Fisher's LSD test, $p = 0.02$, Supplementary Fig. 3c). In contrast, when comparing responses
205 to each type of optic flow, after subtracting the response to stationary stimuli, both the
206 WBAD and WBAS depended strongly on velocity, however, evidence for sexual dimorphism
207 was limited (Fig. 5g, h and Table 1). Indeed, only the WBAS in response to lift showed a
208 significant sex-velocity interaction (Fig. 5g, h and Table 1).

209 The limited extent of sexual dimorphism observed in behaviour (Fig. 5g, h and Table 1)
210 contrasts with the neural responses (Fig. 3e, f and Table 1). Additionally, it is difficult to

211 align the behavioural responses to different types of optic flow with the neuronal input. For
212 example, in response to higher clockwise roll velocities of (100 - 200°/s), hoverflies exhibit a
213 decreased WBAD (positive roll, Fig. 5g) and a slightly increased WBAS (positive roll, Fig.
214 5h) indicating either a leftward turn or an anticlockwise body correction. Similarly, both RHS
215 neuron types give strong responses to clockwise roll (positive roll, Fig. 3e, f). However,
216 sideslip moving leftwards also elicits a decreased WBAD (negative sideslip, Fig. 5g) and an
217 increased WBAS (negative sideslip, Fig. 5h) but neither neuron type responds strongly to this
218 (negative sideslip, Fig. 3e, f).

219 We found that neither lift nor thrust evoke large turning responses (Fig. 5g), however, large
220 and significant increases in the WBAS were observed in hoverflies experiencing the
221 sensation of falling (positive lift, Fig. 5h and Table 1) or being pushed backwards (negative
222 thrust, Fig. 5h and Table 1). Interestingly, each neuron type responds to lift and thrust in a
223 different manner, with OFS DN1 being excited by upwards lift and approaching thrust (Fig.
224 3e), whereas OFS DN2 is excited by downwards lift and receding thrust (Fig. 3f).

225 In electrophysiology we used a horizontally oriented visual monitor (Fig. 1), whereas in
226 behaviour the monitor was rotated 90°[27]. To ensure that this did not substantially affect the
227 shape of the velocity-response functions, we reduced the stimuli to the central square in both
228 behaviour and electrophysiology. This reduction caused a slight but significant change in
229 neuronal (central square; Supplementary Fig. 5a, two-way ANOVA, $p = 0.04$) and
230 behavioural responses (central square; Supplementary Fig. 5b, two-way ANOVA, $p = 0.04$).
231 However, it did not alter the shape of the velocity response function nor produce a significant

232 interaction between velocity and screen size (two-way ANOVA, $p = 0.36$ and 0.49, OFS
233 DN2 and WBAS, respectively).

234 **Response onset varies depending on stimulus type**

235 It has been previously shown that while neuronal responses are fast[25] behavioural responses
236 occur on a much slower time scale and differ depending on stimulus type[32,33]. We here found
237 that there is no significant effect of sex on either neuronal or behavioural response onset (Fig.
238 6, two-way ANOVA, $p = 0.21$, 0.79 and 0.31, OFS DN1, OFS DN2 and WBAS,
239 respectively). However, the onset for roll compared to lift is significantly longer for OFS
240 DN2 and WBAS but not for OFS DN1 (Fig. 6, two-way ANOVA, $p < 0.0001$ for both OFS
241 DN2 and WBAS compared to $p = 0.08$ for OFS DN1).

242 Discussion

243 In the hoverfly, the optics, photoreceptors, and HS cells exhibit clear sexual
244 dimorphism[15,16,18,19]. In line with this, our findings reveal that optic flow sensitive descending
245 neurons also show sexually dimorphic velocity response functions (Fig. 3). Yet, despite the
246 multi-level anatomical and neural sexual dimorphism, the wing beat amplitude remains
247 mostly monomorphic (Fig. 5). Moreover, differences between neural and wing beat
248 amplitude velocity response functions (Fig. 3, 5) and response latency (Fig. 6) highlight the
249 likely involvement of downstream processing mechanisms that could reconcile sex-specific
250 sensory encoding with conserved flight control.

251 Although male hoverflies pursue and capture female conspecifics at high speeds[14], previously
252 reported cruising speeds in both field[23] and indoor settings[24] do not differ between sexes. In
253 addition, the median reported speeds are around 0.3 m/s[23,24], well below the 10 m/s reported
254 during outdoor pursuit[14]. In comparison, our results show limited sex-related differences in
255 WBA in response to optic flow speeds up to 2 m/s (Fig. 5), yet we detected pronounced
256 sexual dimorphism in neural responses at velocities as low as 0.5 m/s (Fig. 3, Table 1). This
257 suggests that sensory processing differences emerge at lower velocities than the velocities
258 where motor output diverges. Moreover, the WBA response latency to roll is much longer
259 that to lift, and much longer than the corresponding neural activity (Fig. 6), implying that
260 temporal integration or additional circuit-level modulation may delay and refine motor
261 execution. Together, these findings suggest a complex transformation between sex-specific
262 sensory encoding and conserved motor behaviour, potentially mediated by downstream
263 integration or additional alternate neural pathways that bypass the descending neurons
264 studied here.

265 Both neurons project broadly within the thoracic ganglion, including in zones associated with
266 prothoracic and pterothoracic nerve input (Fig. 4), suggesting involvement in wing and
267 foreleg motor control. Nevertheless, there is currently no direct evidence implicating them in
268 the control of wingbeat amplitude. Interestingly, DNOVS2 in *Drosophila*, a physiologically
269 similar neuron to OFS DN2[9], has been indirectly linked to rapid turning behaviour[6].
270 Furthermore, silencing HS and VS cells, the presumed presynaptic LPTCs to these
271 descending neurons, results in reductions in WBA only at higher stimulus speeds[34]. These
272 findings suggest that HS and VS cells, along with their downstream targets, may be

specialized for driving fast optomotor responses under high-speed visual motion (>180°/s), rather than broadly regulating WBA across all velocities, including those examined in this study.

Beyond their potential involvement in wingbeat amplitude modulation, OFS DNs may play a role in coordinating head and body positioning during flight, especially in contexts requiring precise visual alignment and rapid manoeuvring. Indeed, the *Drosophila* physiological homologs of OFS DN1 and OFS DN2[9], DNHS1 and DNOVS2, have been implicated in controlling head movements, abdominal ruddering, and engagement with the haltere motor system for flight stabilization[6]. Moreover, the sexual dimorphism in neural responses (Fig. 3) could reflect an evolutionary tuning of visuomotor pathways in males, optimized for fast, directional adjustments rather than gross changes in WBA. For instance, whilst changes in WBAS are similar when generating either lift or thrust (Fig. 5), body pitch dynamically adjusts their ratio, driving behavioural variation[35]. Thus, OFS DNs may serve as integral components of a broader flight control architecture, interfacing optic flow detection with dynamic body and head positioning systems to support complex, sex-specific behavioural outcomes, particularly in males engaging in high-speed pursuits.

Flight speed in insects results from a complex integration of multiple kinematic parameters, not solely from changes in wingbeat amplitude. Many species refine their aerodynamic output by modulating wingbeat frequency, angle of attack, wing tip trajectory, deviations from the mean stroke plane and through precise adjustments to the timing and duration of the up- and downstrokes[36]. These control strategies support agile manoeuvring, particularly

294 during visually guided behaviours such as the high-speed pursuits undertaken by male
295 hoverflies. Furthermore, the smaller body size of male hoverflies compared to females[20,21]
296 may confer biomechanical advantages, including reduced mass, facilitating faster
297 acceleration, heightened responsiveness, and lower metabolic costs for executing flight
298 manoeuvres[22,37], which do not appear in a tethered flight set-up. Such enhanced agility is
299 likely crucial for rapid direction changes required during courtship and may enable male
300 hoverflies to outperform female flies without relying on increased wingbeat amplitude.

301 Taken together, our findings reveal significant differences between sexually dimorphic
302 sensory encoding and conserved motor output in hoverfly flight at cruising speeds. Although
303 OFS DNs and their upstream visual circuits display clear sex-specific tuning, wingbeat
304 amplitude changes in response to optic flow stimuli remain relatively similar between the
305 sexes, suggesting additional mechanisms downstream of sensory input. This likely reflects a
306 complex interplay of biomechanical properties, multisensory integration and circuit-level
307 modulation, each shaping and refining behavioural outcomes to meet distinct demands,
308 preserving the consistency of low-speed manoeuvres whilst enabling sex-specific tuning
309 during high-speed pursuits.

310 Methods

311 Animals

312 For all experiments, male and female *Eristalis tenax* were reared and housed as described
313 previously[21]. Briefly, eggs were collected from females captured under permit in Wittunga

314 Botanic Garden, Adelaide, South Australia. Upon hatching, larvae were reared in a rabbit
315 dung slurry until third instar larvae emerged to pupate. Eclosion occurred 1-2 weeks post-
316 pupation. Adult hoverflies were used for behavioural experiments at 17-87 days post-
317 eclosion, for intracellular electrophysiology and subsequent morphological reconstruction at
318 38-54 days, and for extracellular electrophysiology at 8-204 days.

319 **Electrophysiology**

320 Before recording the animal was immobilised, mounted dorsal side down and secured using a
321 mixture of beeswax and resin. A small region of cuticle was removed at the anterior end of
322 the thorax to expose the cervical connective. If required, any excessive gut or tracheal tissue
323 obstructing the recording site was removed and a small volume of PBS was added to prevent
324 drying within the ventral cavity. A fine wire hook was positioned under the cervical
325 connective for mechanical support, and a silver wire was inserted into the cavity to serve as a
326 reference electrode and grounding wire[9].

327 For extracellular recordings, a sharp tungsten microelectrode (2 MΩ, polyimide-insulated;
328 Microprobes) was inserted into the cervical connective[9]. Signals were amplified 1000 times
329 and band-pass filtered between 10–3000 Hz using a DAM50 differential amplifier (World
330 Precision Instruments), followed by noise reduction with a HumBug (Quest Scientific). Data
331 were digitized via a PowerLab 4/30 interface (ADInstruments) and acquired at 40 kHz. Spike
332 sorting was performed in LabChart 7 Pro (ADInstruments) based on the amplitude and width
333 of individual action potentials.

334 For intracellular recordings, aluminosilicate electrodes were pulled using a Sutter P-1000
335 micropipette puller, achieving a resistance of approximately 40-70 MΩ. Electrode tips were
336 filled with 3% neurobiotin (Vector Laboratories), then backfilled with 1 M KCl using a
337 syringe, leaving a small air bubble between the two solutions. Electrodes were inserted into
338 the cervical connective for recording, and the resulting signal was amplified using an
339 Axoclamp-2B amplifier (Axon Instruments), followed by 50 Hz noise reduction with a
340 HumBug (Quest Scientific). Data acquisition and digitization were performed at 10 kHz
341 using an NI USB-6210 16-bit data acquisition card (National Instruments) and the MATLAB
342 Data Acquisition Toolbox (Mathworks), using in house software
343 (https://github.com/HoverflyLab/SampSamp).

344 **Morphological reconstructions**

345 Following intracellular recordings, neurons were stained iontophoretically with neurobiotin
346 using currents in the 1 nA range for 3–12 minutes. The nervous system was then carefully
347 dissected and fixed in 4% paraformaldehyde overnight. Tissue was incubated with a Cy3-
348 streptavidin conjugate (1:100; Jackson ImmunoResearch) for 2 hours, then dehydrated
349 through an ethanol series (50–100%) for 15-20 minutes per step. After washing in PBT, the
350 tissue was cleared in RapiClear (SUNJIN Lab) and mounted with spacers. Imaging was
351 performed using a Zeiss LSM 880 Fast Airyscan confocal microscope at the institutional
352 microscopy facility. Neuron morphology and cervical connective width were quantified using
353 ImageJ[38].

354

Tethered flight

Prior to flight recordings, hoverflies were tethered at a 32° angle using a beeswax–resin mixture to a small pin inserted into a hypodermic needle (BD Microlance, 23G × 1¼"). Flight was initiated by manually providing airflow for 1–10 minutes until consistent flight behaviour was observed. Once positioned at the centre of the flight arena, hoverflies were filmed from above at 100 Hz using a Sony PlayStation 3 Move Eye Camera (SLEH- 00448, Sony) with the IR filter removed, and equipped with an infrared pass filter (R72 INFRARED, 49 mm, HOYA; for details see Ref[27]). Illumination was provided by infrared LEDs inserted into USB lights (JANSJÖ LED USB lamp, IKEA) and a Musou Black (Shin Kokushoku Musou black, KOYO Orient Japan) surface was placed beneath the hoverfly to enhance contrast and minimize optical interference.

We used DeepLabCut (DLC) version 2.3.3[26] to train a model to track the thorax, and the peak downstroke angle, referred to as the wing beat amplitude (WBA), of the left and right wing (WBA_L and WBA_R; Fig. 5a, b), as described previously[27]. Briefly, we manually labelled six anatomical landmarks: the tegula and wing tip of both left and right wing, the anterior thorax, and the anterior abdomen (Fig. 5a, b), across 16 extracted video frames per individual from four hoverflies (2 males, 2 females). In addition to examples where the hoverfly was not flying, these frames included responses to yaw rotation and forward translation. The DLC model was trained for 300,000 iterations, yielding train and test errors of 1.2 and 1.16 pixels, respectively.

To identify potential tracking errors from DLC, we smoothed the WBA time series using MATLAB's *smooth* function with both *loess* and *rloess* methods. Because *rloess* is more resistant to outliers, we used it to detect abnormal data points. For each wing, if the absolute difference between the *loess*- and *rloess*-smoothed signals exceeded 5% for more than 1 s, the data were excluded due to suspected tracking artifacts. The smoothing was used only for error detection; all subsequent analyses were performed on the unsmoothed data. In addition, we excluded data if the WBA of either wing dropped below 40° for at least 0.5 s, as this indicated a cessation of flight. Finally, entire trials were excluded if the hoverfly was not flying for more than 50% of the trial duration.

Visual stimuli

Visual stimuli were generated using custom software (https://github.com/HoverflyLab/FlyFly/releases/tag/v4.2.3) written in MATLAB, incorporating the Psychophysics Toolbox[39,40]. All screens had a refresh rate of 165 Hz and a linearized contrast with a mean illuminance of 200 Lux. For intracellular recordings, the hoverfly was placed 13 cm away from a ViewSonic screen with a resolution of 2560 × 1440 pixels, corresponding to 143° × 107° of the visual field. For extracellular recordings, the hoverfly was placed 6.5 cm away from a 2560 × 1440 pixel Asus screen, yielding a projected visual field of 155° × 138°. For behavioural recordings, the hoverfly was placed 10 cm from a vertically orientated Asus screen (1440 × 2560 pixel) producing a projected size of 118° × 142°. To evaluate the impact of different screen orientations in electrophysiology and

395 behaviour, visual stimuli were presented either full-screen or using the central 1440 × 1440
396 pixel square (Supplementary Fig. 5).

397 *Receptive field mapping*

398 To map each neuron's receptive field, we presented local sinusoidal gratings (average 38 ×
399 38°) drifting in 8 directions for 0.36 s each, across 48 overlapping locations, as previously[9].
400 Stimuli were full contrast, with an average spatial frequency of 0.14 cycles/° and a temporal
401 frequency of 5 Hz. At each location, we calculated the local maximum spike frequency (red,
402 inset, Fig. 1b, e). After subtracting the spontaneous rate, calculated for 0.8 s preceding
403 stimulus onset (dotted, inset, Fig. 1b, e), we spatially interpolated the resulting local
404 maximum responses 10 times (colour coding, Fig. 1a, d). Receptive field centres (red circle,
405 Fig. 1b, e) and sizes (Supplementary Fig. 1f) were defined using the resulting 50% contour
406 line (black, Fig. 1b, e). As recordings were performed with the animal ventral side up,
407 receptive fields were rotated to display them with the dorsal side up (Supplementary Fig. 2a).

408 Next, at each location, we fit a cosine function to the responses to the different directions of
409 motion, to extract the local preferred direction (LPD) and local motion sensitivity (LMS;
410 inset, Fig. 1c, f). These were visualized as vectors where angle indicates LPD and length
411 indicates LMS (arrows, Fig. 1a, d). We defined the receptive field preferred direction as the
412 median of LPDs at locations where LMS exceeded 50% of the maximum (black and red
413 arrows; Fig. 1c, f), using circ_median from the CircStat toolbox for MATLAB[41]. We
414 calculated the LPD variance using the circ_var functions from CircStat toolbox for

415 MATLAB[41], of LPDs at locations where LMS exceeded 50% of the maximum (black and red
416 arrows; Fig. 1c, f).

417 We extracted unpublished receptive field data from 100 reference neurons (other data from 5
418 of these optic flow sensitive descending neurons has been published previously[42]) to set
419 exclusion criteria (red shading, Supplementary Fig. 1a, b and c) and to classify the OFS DNs
420 used in the rest of this study. OFS DN1 LHS neurons were defined by receptive field
421 preferred directions between 120° and 200° (light green, Fig. 1g). OFS DN1 RHS neurons
422 were defined by receptive field preferred directions between 340° and 60° (dark green, Fig.
423 1g). OFS DN2 neurons were classified by receptive field preferred directions between 220°
424 and 320° (yellow and orange, Fig. 1g), with the location of the receptive field centre relative
425 to the midline determining whether they were LHS or RHS (yellow and orange, Fig. 1h).

426 *Directional sensitivity*

427 Full-screen sinusoidal gratings were presented at full contrast, using the same spatial (0.14
428 cycles/°) and temporal (5 Hz) frequencies as in receptive field mapping. Directional
429 responses were rotated to account for the ventral-side-up recording position, and data from
430 LHS neurons were mirrored across the midline to display all neurons as RHS (Supplementary
431 Fig 2a). For each stimulus direction, mean spike frequency was calculated over the stimulus
432 duration, excluding the first 100 ms to avoid onset transients[43]. A cosine function was fit to
433 these responses, to extract its amplitude and preferred direction (Supplementary Fig 2b).

434

Responses to optic flow

We used a starfield stimulus to generate the type of perspective-corrected optic flow that would have been seen by the hoverfly if it was moving through a space of 2 cm diameter spheres (for details, see Ref[9,25]). These simulated translations at 0.5 m/s (sideslip, lift, and thrust, Supplementary movie 2) or rotations (pitch, yaw, and roll, Supplementary movie 1), at 50°/s. To quantify neural responses, the mean spike frequency was calculated over the 0.97 s stimulus duration, excluding the first 0.1 s to avoid onset-related transients[43]. The spontaneous firing rate, averaged across 0.48 s immediately preceding stimulus onset (circles, Supplementary Fig 3a, b), was subtracted from the response.

Velocity response functions

We used four types of optic flow: three translations (sideslip, lift and thrust) and one rotation (roll). Translations were presented at velocities of −2, −1.5, −1, −0.4, −0.2, −0.1, 0, 0.1, 0.2, 0.4, 1, 1.5, and 2 m/s, while rotations were presented at 200, −150, −100, −40, −20, −10, 0, 10, 20, 40, 100, 150, and 200°/s. The sign of the velocity indicates the direction of motion as seen by the fly when corrected for its position, with positive values corresponding to counterclockwise roll, leftward sideslip, downward lift, and thrust moving away. Conversely, negative values indicate clockwise roll, rightward sideslip, upward lift, and thrust moving toward the hoverfly. The upper limit was defined by the movement of the individual dots within the starfield stimulus between frames, i.e. was limited by the refresh rate of the screen.

Each trial consisted of 39 stimuli (13 unique velocities × 3 repetitions), presented in a random order, with each stimulus lasting 2 s, immediately followed by the next velocity. Trials began with a 1 s blank screen, which served as the pre-stimulation baseline (Fig. 3a and Fig. 5a). Each optic flow condition was repeated multiple times, resulting in at least nine repetitions for each velocity and neuron, and five repetitions for each velocity and animal in behaviour.

For neuronal recordings, velocity response function trials were interleaved with the optic flow stimuli described above. In behavioural experiments, a flight refresher sequence interspersed each velocity tuning trial. This consisted of sinusoidal gratings (200° wavelength, 5 Hz) drifting rightward, leftward, and rightward again for 4 s each.

Neural responses were quantified as the mean spike frequency during the final second of stimulation (grey shaded areas, Fig. 3a–c). We then calculated the median across trials for each velocity (Fig. 3d). Pre-stimulation activity (spontaneous rate) was measured over a 2 s window immediately preceding stimulus onset. In behavioural experiments, we extracted the mean wing beat amplitude of the left and right wings ($\overline{WBA_L}$, $\overline{WBA_R}$, Fig. 5b) during the final second of stimulation (grey shaded areas, in Fig. 5 c, d and e). For each velocity, we calculated the WBA difference (WBAD, defined as $\overline{WBA_L} - \overline{WBA_R}$) and the WBA sum (WBAS, defined as $\overline{WBA_L} + \overline{WBA_R}$, Fig. 5b). We then calculated the median across repetitions for each individual (Fig. 5f). Pre-stimulation responses were averaged over a 0.5 s time window immediately preceding stimulus onset.

Response onset

For neuronal recordings, we compared onset times for clockwise roll (+50°/s) and either upwards lift (+0.5 m/s) for OFS DN 1 or downwards lift (-0.5 m/s) for OFS DN2, stimuli which generated strong responses in these neurons (Fig. 3 e, f). Mean spike frequency was calculated over the stimulus duration, excluding the first 0.1 s to avoid onset transients[43]. Onset was defined as the first time point after the first 0.1 s, where spike rate exceeded 80% of the mean.

For behaviour, we used responses to roll (-200°/s) and lift (+2 m/s). Mean WBAS was defined as the average response during the final second of stimulation, and onset was defined as the first time point where WBAS exceeded 80% of this mean.

Data availability and statistics

All data and analysis scripts have been submitted to DataDryad (private link for peer review: doi:10.5061/dryad.tb2rbp0fd).

Throughout the text n refers to individual repetitions, whereas N refers to individual neurons (electrophysiology) or animals (behaviour). All data are presented as median and interquartile range, unless otherwise indicated.

Statistical analyses were performed in Prism 10.4 (GraphPad Software), except for circular statistics, which were conducted using the CircStat toolbox for MATLAB[41]. The results of the statistical tests are given in figure legends and in Table 1.

Acknowledgements

We thank Biomedical Engineering at SAHLN and the Botanic Gardens of Adelaide for their ongoing support. This research was funded by the US Air Force Office of Scientific Research (AFOSR, FA9550-19-1-0294 and FA9550-23-1-0473) and the Australian Research Council (ARC, DP210100740, DP230100006 and DP250104770).

Declaration of interests

The authors declare no competing interests.

References

1 Mauss, A. S. & Borst, A. Optic flow-based course control in insects. *Curr Opin Neurobiol* **60**, 21-27, doi:10.1016/j.conb.2019.10.007 (2020).

2 Franz, M. O. & Krapp, H. G. Wide-field, motion-sensitive neurons and matched filters for optic flow fields. *Biol Cybern* **83**, 185-197 (2000).

3 Krapp, H. G., Hengstenberg, B. & Hengstenberg, R. Dendritic structure and receptive-field organization of optic flow processing interneurons in the fly. *J Neurophysiol* **79**, 1902-1917. (1998).

4 Haikala, V., Joesch, M., Borst, A. & Mauss, A. S. Optogenetic control of fly optomotor responses. *J Neurosci* **33**, 13927-13934, doi:10.1523/jneurosci.0340-13.2013 (2013).

5 Pokusaeva, V. O., Satapathy, R., Symonova, O. & Joesch, M. Bilateral interactions of optic-flow sensitive neurons coordinate course control in flies. *Nat Commun* **15**, 8830, doi:10.1038/s41467-024-53173-w (2024).

6 Suver, M. P., Huda, A., Iwasaki, N., Safarik, S. & Dickinson, M. H. An Array of Descending Visual Interneurons Encoding Self-Motion in Drosophila. *J Neurosci* **36**, 11768-11780, doi:10.1523/JNEUROSCI.2277-16.2016 (2016).

7 Erginkaya, M. *et al.* A competitive disinhibitory network for robust optic flow processing in Drosophila. *bioRxiv*, 2023.2008.2006.552150, doi:10.1101/2023.08.06.552150 (2023).

8 Namiki, S., Dickinson, M. H., Wong, A. M., Korff, W. & Card, G. M. The functional organization of descending sensory-motor pathways in *Drosophila*. *eLife* **7**, e34272, doi:10.7554/eLife.34272 (2018).

9 Nicholas, S., Leibbrandt, R. & Nordström, K. Visual motion sensitivity in descending neurons in the hoverfly. *J Comp Physiol A* **206**, 149-163, doi:10.1007/s00359-020-01402-0 (2020).

527 10 Haag, J., Wertz, A. & Borst, A. Integration of lobula plate output signals by
528 DNOVS1, an identified premotor descending neuron. *J Neurosci* **27**, 1992-2000,
529 doi:10.1523/jneurosci.4393-06.2007 (2007).
530 11 Wertz, A., Borst, A. & Haag, J. Nonlinear integration of binocular optic flow by
531 DNOVS2, a descending neuron of the fly. *J Neurosci* **28**, 3131-3140,
532 doi:10.1523/jneurosci.5460-07.2008 (2008).
533 12 Collett, T. S. & Land, M. F. Visual control of flight behaviour in the hoverfly, *Syritta*
534 *pipiens* L. *J Comp Physiol A* **99**, 1-66 (1975).
535 13 Wellington, W. & Fitzpatrick, S. Territoriality in the drone fly, *Eristalis tenax*
536 (Diptera, Syrphidae). *Can Entomol* **113**, 695-704 (1981).
537 14 Collett, T. S. & Land, M. F. How hoverflies compute interception courses. *Journal of*
538 *comparative physiology* **125**, 191-204, doi:10.1007/BF00656597 (1978).
539 15 Straw, A. D., Warrant, E. J. & O'Carroll, D. C. A 'bright zone' in male hoverfly
540 (*Eristalis tenax*) eyes and associated faster motion detection and increased contrast
541 sensitivity. *J Exp Biol* **209**, 4339-4354, doi:10.1242/jeb.02517 (2006).
542 16 van Hateren, J. H., Hardie, R. C., Rudolph, A., Laughlin, S. B. & Stavenga, D. G. The
543 bright zone, a specialized dorsal eye region in the male blowfly *Chrysomyia*
544 *megacephala*. *J Comp Physiol A* **164**, 297-308 (1989).
545 17 Hornstein, E. P., O'Carroll, D. C., Anderson, J. C. & Laughlin, S. B. Sexual
546 dimorphism matches photoreceptor performance to behavioural requirements. *Proc R*
547 *Soc Lond B Biol Sci* **267**, 2111-2117., doi:10.1098/rspb.200.1257 (2000).
548 18 Nordström, K., Barnett, P. D., Moyer de Miguel, I. M., Brinkworth, R. S. A. &
549 O'Carroll, D. C. Sexual dimorphism in the hoverfly motion vision pathway. *Curr Biol*
550 **18**, 661-667, doi:10.1016/j.cub.2008.03.061 (2008).
551 19 Barnett, P. D., Nordström, K. & O'Carroll, D. C. Motion adaptation and the velocity
552 coding of natural scenes. *Curr Biol* **20**, 994-999, doi:10.1016/j.cub.2010.03.072
553 (2010).

20 Dankova, K., Nicholas, S. & Nordstrom, K. Temperature during pupal development affects hoverfly developmental time, adult life span, and wing length. *Ecol Evol* **13**, e10516, doi:10.1002/ece3.10516 (2023).

21 Nicholas, S., Thyselius, M., Holden, M. & Nordström, K. Rearing and long-term maintenance of *Eristalis tenax* hoverflies for research studies. *JoVE*, e57711, doi:doi:10.3791/57711 (2018).

22 Dudley, R. Mechanisms and implications of animal flight maneuverability. *Integr Comp Biol* **42**, 135-140, doi:10.1093/icb/42.1.135 (2002).

23 Thyselius, M., Gonzalez-Bellido, P. T., Wardill, T. J. & Nordstrom, K. Visual approach computation in feeding hoverflies. *J Exp Biol* **221**, doi:10.1242/jeb.177162 (2018).

24 Thyselius, M. *et al.* Hoverfly (Eristalis tenax) pursuit of artificial targets. *J Exp Biol* **226**, doi:10.1242/jeb.244895 (2023).

25 Leibbrandt, R., Nicholas, S. & Nordström, K. The impulse response of optic flow-sensitive descending neurons to roll m-sequences. *J Exp Biol* **224**, doi:10.1242/jeb.242833 (2021).

26 Mathis, A. *et al.* DeepLabCut: markerless pose estimation of user-defined body parts with deep learning. *Nat Neurosci* **21**, 1281-1289, doi:10.1038/s41593-018-0209-y (2018).

27 Ogawa, Y. *et al.* Combining Unity with machine vision to create low latency, flexible and simple virtual realities. *Methods in Ecology and Evolution* **16**, 126-144, doi:https://doi.org/10.1111/2041-210X.14449 (2025).

28 Götz, K. G. Flight control in *Drosophila* by visual perception of motion. *Kybernetik* **4**, 199-208 (1968).

29 Maimon, G., Straw, A. D. & Dickinson, M. H. Active flight increases the gain of visual motion processing in *Drosophila*. *Nat Neurosci* **13**, 393-399, doi:nn.2492 [pii] 10.1038/nn.2492 [doi] (2010).

30 Tammero, L. F., Frye, M. A. & Dickinson, M. H. Spatial organization of visuomotor reflexes in Drosophila. *J Exp Biol* **207**, 113-122, doi:10.1242/jeb.00724 (2004).

31 Ristroph, L. *et al.* Discovering the flight autostabilizer of fruit flies by inducing aerial stumbles. *Proc Natl Acad Sci U S A* **107**, 4820-4824, doi:10.1073/pnas.1000615107 (2010).

32 Schnell, B., Weir, P. T., Roth, E., Fairhall, A. L. & Dickinson, M. H. Cellular mechanisms for integral feedback in visually guided behavior. *Proc Natl Acad Sci U S A* **111**, 5700-5705, doi:1400698111 [pii] 10.1073/pnas.1400698111 [doi] (2014).

33 Theobald, J. C., Ringach, D. L. & Frye, M. A. Dynamics of optomotor responses in *Drosophila* to perturbations in optic flow. *J Exp Biol* **213**, 1366-1375, doi:213/8/1366 [pii] 10.1242/jeb.037945 [doi] (2010).

34 Kim, A. J., Fenk, L. M., Lyu, C. & Maimon, G. Quantitative Predictions Orchestrate Visual Signaling in Drosophila. *Cell* **168**, 280-294 e212, doi:10.1016/j.cell.2016.12.005 (2017).

35 Zanker, J. M. The Wing Beat of Drosophila-Melanogaster .3. Control. *Philos T R Soc B* **327**, 45-64, doi:DOI 10.1098/rstb.1990.0042 (1990).

36 Sane, S. P. The aerodynamics of insect flight. *Journal of Experimental Biology* **206**, 4191-4208, doi:10.1242/jeb.00663 (2003).

37 Niven, J. E. & Scharlemann, J. P. W. Do insect metabolic rates at rest and during flight scale with body mass? *Biol Letters* **1**, 346-349, doi:10.1098/rsbl.2005.0311 (2005).

38 Schneider, C. A., Rasband, W. S. & Eliceiri, K. W. NIH Image to ImageJ: 25 years of image analysis. *Nat Methods* **9**, 671-675, doi:10.1038/nmeth.2089 (2012).

39 Brainard, D. H. The Psychophysics Toolbox. *Spat Vis* **10**, 433-436 (1997).

40 Pelli, D. G. The VideoToolbox software for visual psychophysics: transforming numbers into movies. *Spat Vis* **10**, 437-442 (1997).

41 Berens, P. CircStat: A MATLAB toolbox for circular statistics. *Journal of Statistical Software* **31**, 1 - 21, doi:10.18637/jss.v031.i10 (2009).

42 Nicholas, S. & Nordström, K. Facilitation of neural responses to targets moving against optic flow. *Proc Natl Acad Sci U S A* **118**, doi:10.1073/pnas.2024966118 (2021).

43 Nicholas, S. & Nordstrom, K. Persistent Firing and Adaptation in Optic-Flow-Sensitive Descending Neurons. *Curr Biol* **30**, 2739-2748 e2732, doi:10.1016/j.cub.2020.05.019 (2020).

44 Kane, G. A., Lopes, G., Saunders, J. L., Mathis, A. & Mathis, M. W. Real-time, low-latency closed-loop feedback using markerless posture tracking. *eLife* **9**, doi:10.7554/eLife.61909 (2020).

Figure legends

Fig. 1. Classification of optic flow sensitive (OFS) descending neurons (DN) in *Eristalis tenax*. a Receptive field of a representative OFS DN1 recorded from a male hoverfly. Colour coding indicates the local maximum spike frequency, and the direction of the arrows shows the local preferred direction (LPD) and their length the local motion sensitivity (LMS). **b** Contour line representing the 50% receptive field boundary based on local maximum spike frequency from panel a. Inset: example response at one central location to eight directions of motion (black circles), showing local maximum spike frequency (local max, red line) above spontaneous rate (spont, black dotted line). **c** Preferred direction map of the same example neuron at locations where local motion sensitivity (LMS) exceeds 50% of the maximum (red arrow). Inset: example response at one location to eight directions of motion with a sinusoidal fit (black line), illustrating LMS (red line) and LPD (red open arrowhead). **d** Receptive field of a representative male OFS DN2. **e** 50% receptive field contour and receptive field centre of the neuron shown in panel d. **f** Preferred direction map of the same OFS DN2. **g** Distribution of receptive field preferred directions across 100 male reference neurons, colour-coded by neuron classification. Dashed lines in corresponding colours indicate the thresholds used for neuron type classification. **h** Receptive field centres of the same 100 reference neurons, using the same colour coding. **i** Relationship between preferred direction and receptive field centre for the 100 neurons.

Fig. 2. Sex-based comparison of direction sensitivity in OFS DNs. a Polar plot showing the preferred direction of male (blue) and female (red) OFS DNs in response to a full-screen,

643 full-contrast sinusoidal grating (spatial wavelength 7º, temporal frequency 5 Hz). Individual
644 data points represent the response amplitude and preferred direction of each OFS DN. Larger,
645 salient circles indicate the population median, with error bars showing the interquartile range.
646 The dashed lines indicate the directional thresholds used to classify neuron type, as OFS DN1
647 (male: N = 9; female: N = 12) or OFS DN2 (male: N = 20; female: N = 14). Asterisk
648 indicates a statistically significant difference ($p < 0.05$), Watson-Williams two-sample test. **b**
649 Comparison of male and female OFS DN1 responses to translational optic flow at 0.5 m/s:
650 sideslip, lift and thrust; and rotational optic flow at 50 º/s: pitch, yaw and roll (male: N = 9;
651 female: N = 12). **c** Comparison of male and female OFS DN2 responses to the same optic
652 flow stimuli (male: N = 20; female: N = 14). Data presented as median and interquartile
653 range.

654 **Fig. 3. Velocity response functions in male and female OFS DNs. a** Example stimulus
655 profile over time, with roll velocity on the y-axis. **b** Representative spike histogram from a
656 single trial from a male OFS DN2, smoothed using a 100 ms square-wave filter with 0.025
657 ms resolution, and time-aligned to the stimulus shown in panel a. Grey shading in panels a
658 and b highlight the analysis windows used to calculate response. **c** Example extracellular raw
659 data traces extracted from the analysis windows in panel b, illustrating neuronal responses to
660 roll velocities of –150, 10, and 200 º/s. **d** Average spike frequency (grey circles) was
661 calculated for each repetition from each neuron (N = 1 neuron, n = 18 repetitions), and the
662 median of these (black) was used for further analysis. **e** Velocity response functions of OFS
663 DN1 in male (blue) and female (red) hoverflies in response to roll (N = 4 males, 5 females),
664 sideslip (N = 5, 6), lift (N = 4, 4), and thrust (N = 3, 5). **f** Velocity response functions of OFS

665 DN2 to roll (N = 10 males, 8 females), sideslip (N = 6, 7), lift (N = 6, 7), and thrust (N = 6,
666 7). Data in panels e and f are presented as median and interquartile range. Asterisks indicate
667 statistically significant differences, two-way ANOVA with Šídák's multiple comparisons test
668 (** $p < 0.01$ and **** $p < 0.0001$), see also Table 1.

669 **Fig. 4. Morphological reconstruction of OFS DNs. a** Schematic diagram of the hoverfly
670 central brain and thoracic ganglia showing the projections of OFS DN1 (green) and OFS
671 DN2 (orange). Key anatomical landmarks are labelled: OL, optic lobe; CB, central brain; CC,
672 cervical connective; T1 LN, prothoracic leg nerve; T2 LN, mesothoracic leg nerve; T3 LN,
673 metathoracic leg nerve; TAG, thoracic-abdominal ganglion; FN, frontal nerve; PtN,
674 pterothoracic nerve; HN, haltere nerve; AbN, abdominal nerve. **b** Confocal image of a
675 reconstructed male OFS DN2. White boxes indicate regions magnified in panels c and d**. c**
676 Input dendrites of OFS DN2 around the sub-oesophageal ganglion. **d** Output projections of
677 the same OFS DN2 neuron within the thoracic ganglia. **e** Input dendrites of a female OFS
678 DN2. **f** Output projections of the same neuron. **g** Input dendrites of a male OFS DN1. **h**
679 Output projections from the same neuron.

680 **Fig. 5. WBA velocity response functions in male and female hoverflies. a** Screenshot from
681 a video labelled with trained DeepLabCut models[26,27,44]. Coloured dots correspond to those in
682 panel b, used to extract the wing beat amplitude (WBA). **b** Pictogram illustrating a higher
683 wing beat amplitude on the left wing (WBA_L) compared to the right wing (WBA_R),
684 suggesting a turn to the right. Equations used to calculate wing beat amplitude difference
685 (WBAD) and wing beat amplitude sum (WBAS). **c** Example stimulus with sideslip velocity

686 on the y-axis. **d** Representative WBA for the left (pale colour) and right (salient colour)
687 wings from a single trial, time-aligned with the stimulus shown in panel c. Grey shading in
688 panels c and d indicate the analysis windows used to calculate WBAD and WBAS. **e**
689 Magnified view of example WBA, showing behavioural responses to sideslip velocities of -2,
690 0.2, and 2 m/s. **f** Average WBAS (grey circles) calculated across repetitions (N = 1 animal, n
691 = 19-36 repetitions). Black circles represent the median WBAS per stimulus condition, used
692 for further analysis. **g** WBAD in male (blue) and female (red) hoverflies in response to
693 different optic flow velocities: roll (N = 5 males, 7 females), sideslip (N = 6, 6), lift (N = 7,
694 5), and thrust (N = 6, 5). **h** WBAS to the same stimuli in the same animals. Data in panels g
695 and h are presented as median and interquartile range.

696 **Fig. 6. Response onset to roll and lift stimuli in male and female hoverflies. a** Time to
697 response onset in OFS DN1 to roll (+50 º/s) or lift (+0.5 m/s) stimuli in males (blue, N = 5)
698 and females (red, N = 8). **b** Response onset in OFS DN2 to roll (+50 º/s) or lift (-0.5 m/s)
699 measured in males (N = 20) and females (N = 14). **c** Onset of WBAS responses to roll (-200
700 º/s) and lift (+2 m/s) in males (N = 5 for roll, 9 for lift) and females (N = 7 for roll, 5 for lift).
701 Data are presented as individual repeats with lines indicating median. Asterisks indicate
702 statistically significant differences, two-way ANOVA with uncorrected Fisher's LSD test
703 (** $p < 0.01$ and *** $p < 0.001$).

704 **Table 1. Statistical summary of neural and behavioural velocity response functions.**
705 Results from two-way ANOVA analyses evaluating the effects of stimulus velocity and sex

706 on both neural (OFS DN1 and DN2) and behavioural (WBAS and WBAD) responses.

707 Asterisks denote levels of statistical significance: *** $p < 0.001$, **** $p < 0.0001$.

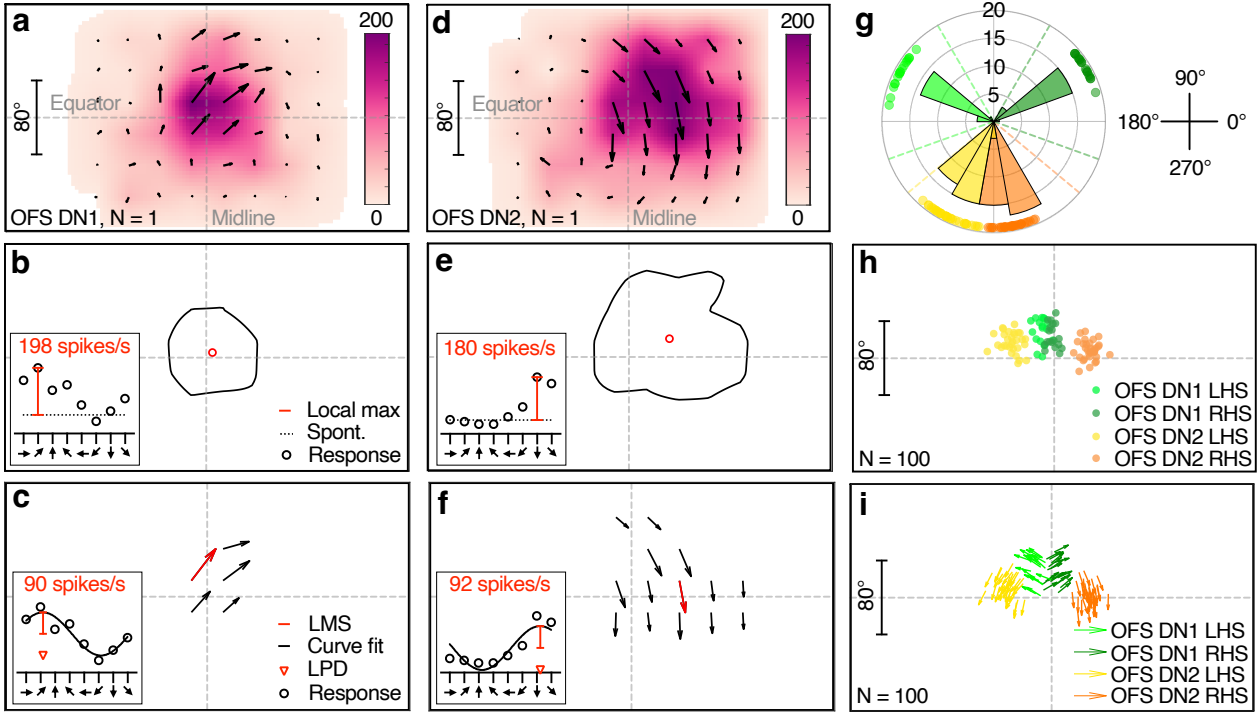
a
200
0
80°
Equator
OFS DN1, N = 1
Midline
d
200
0
80°
Equator
OFS DN2, N = 1
Midline
g
20
15
10
5
90°
180°
0°
270°
b
198 spikes/s
Local max
Spont.
Response
e
180 spikes/s
h
80°
OFS DN1 LHS
OFS DN1 RHS
OFS DN2 LHS
OFS DN2 RHS
N = 100
c
90 spikes/s
LMS
Curve fit
LPD
Response
f
92 spikes/s
i
80°
OFS DN1 LHS
OFS DN1 RHS
OFS DN2 LHS
OFS DN2 RHS
N = 100

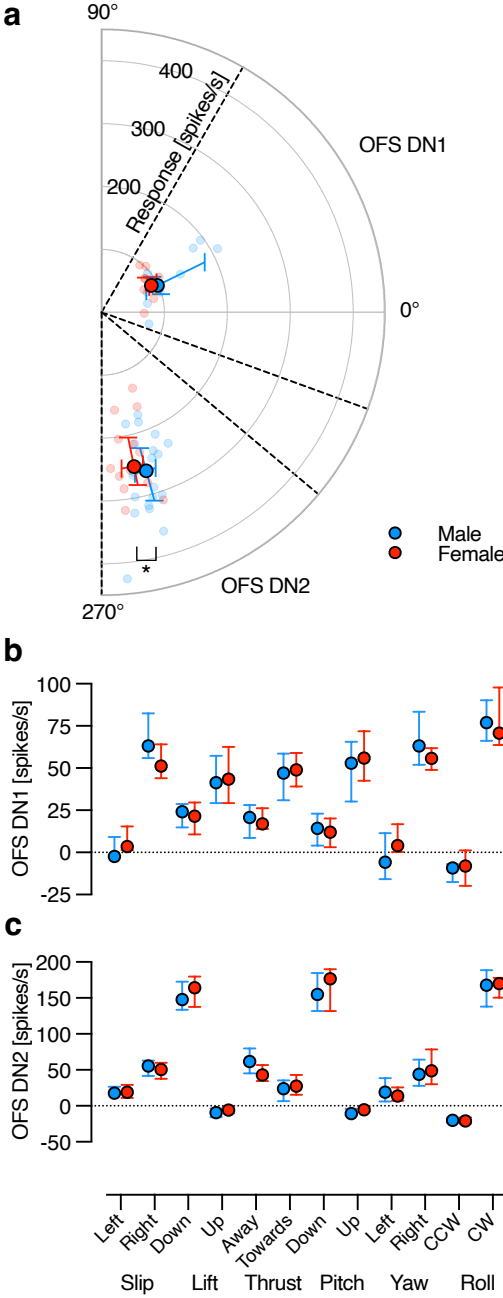
a
90°
400
300
200
Response [spikes/s]
OFS DN1
0°
Male
Female
*
OFS DN2
270°
b
OFS DN1 [spikes/s]
100
75
50
25
0
-25
c
OFS DN2 [spikes/s]
200
150
100
50
0
-50
Left
Right
Down
Up
Away
Towards
Down
Up
Left
Right
CCW
CW
Slip
Lift
Thrust
Pitch
Yaw
Roll

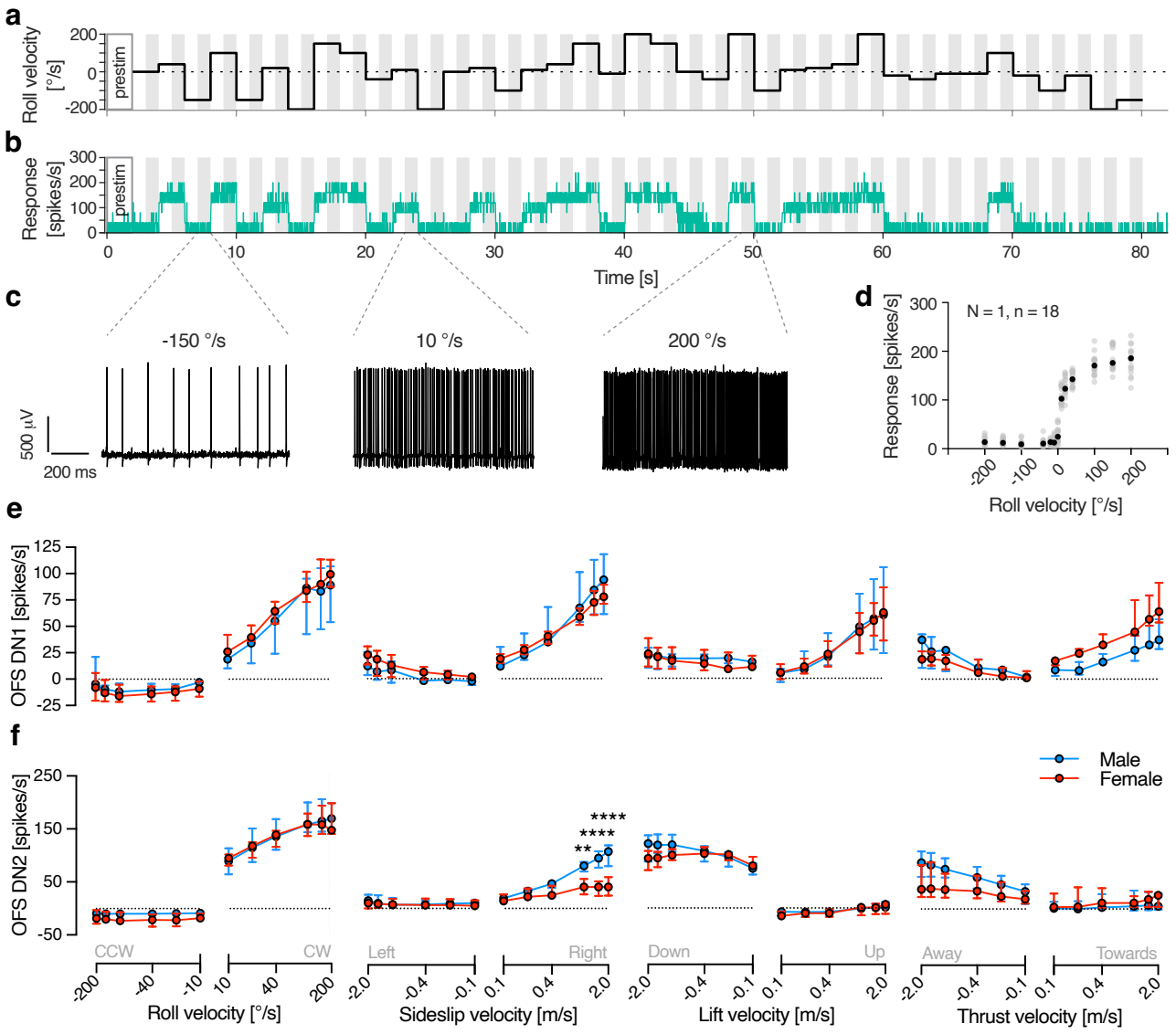
a
Roll velocity [°/s]
200
0
-200
prestim
b
Response [spikes/s]
300
200
100
0
prestim
0
10
20
30
40
50
60
70
80
Time [s]
c
-150 °/s
10 °/s
200 °/s
500 µV
200 ms
d
N = 1, n = 18
Response [spikes/s]
300
200
100
0
-200
-100
0
100
200
Roll velocity [°/s]
e
OFS DN1 [spikes/s]
125
100
75
50
25
0
-25
f
Male
Female
OFS DN2 [spikes/s]
250
150
50
-50
****
****
**
CCW
CW
Left
Right
Down
Up
Away
Towards
-200
-40
-10
10
40
200
-2.0
-0.4
-0.1
0.1
0.4
2.0
Roll velocity [°/s]
Sideslip velocity [m/s]
Lift velocity [m/s]
Thrust velocity [m/s]

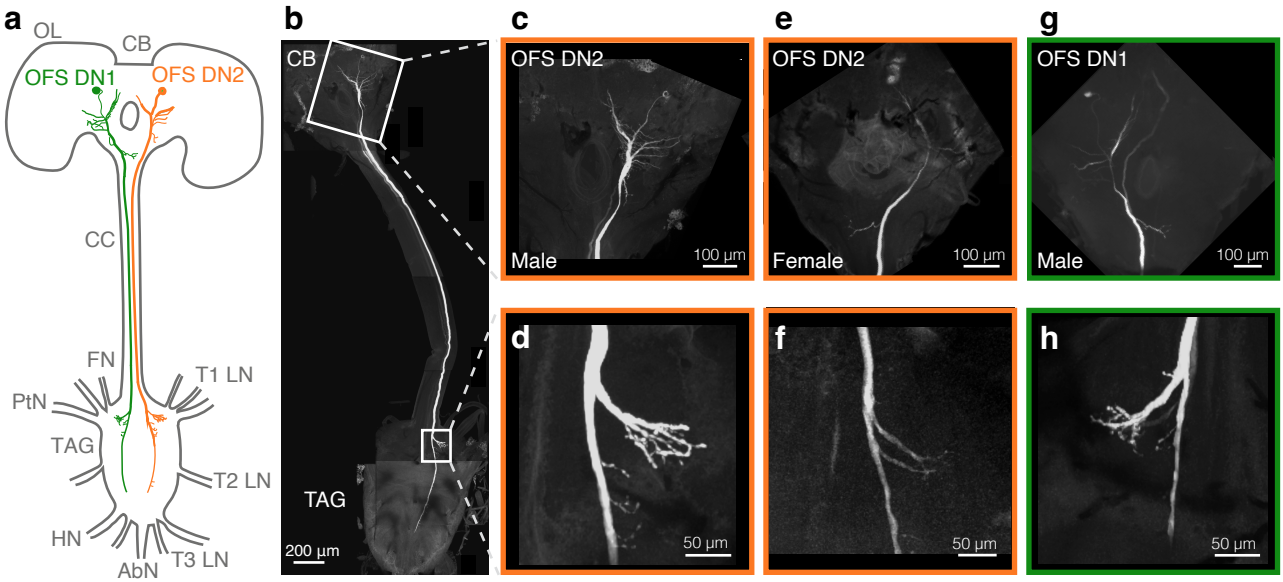
a
OL
CB
OFS DN1
OFS DN2
CC
FN
T1 LN
PtN
TAG
T2 LN
HN
T3 LN
AbN
b
CB
TAG
200 µm
c
OFS DN2
Male
100 µm
e
OFS DN2
Female
100 µm
g
OFS DN1
Male
100 µm
d
50 µm
f
50 µm
h
50 µm

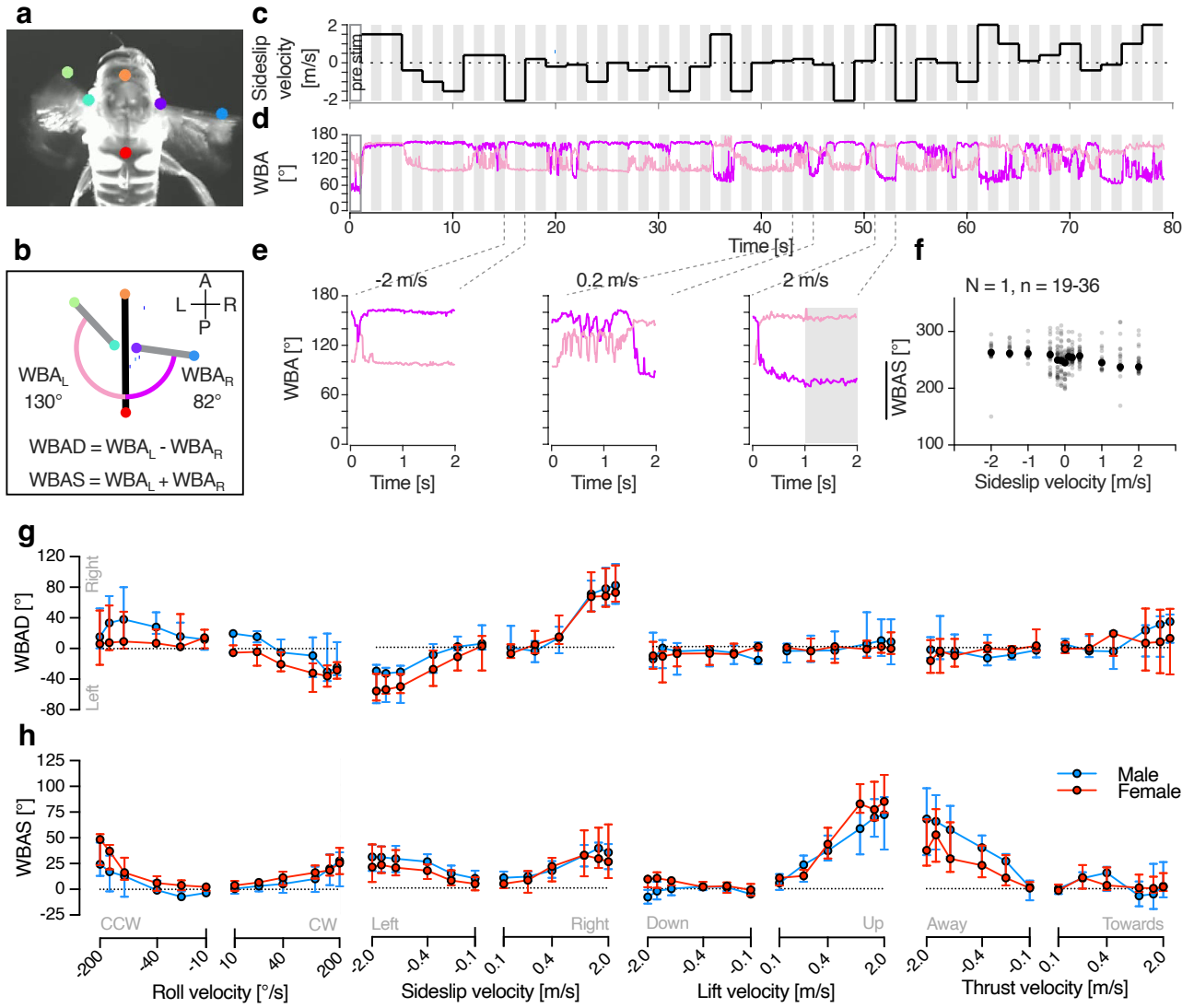
a
b
c
d
e
f
g
h
Sideslip velocity [m/s]
pre stim
WBA [°]
Time [s]
-2 m/s
0.2 m/s
2 m/s
N = 1, n = 19-36
WBAS [°]
Sideslip velocity [m/s]
A
L
R
P
WBA_L 130°
WBA_R 82°
WBAD = WBA_L - WBA_R
WBAS = WBA_L + WBA_R
WBAD [°]
Right
Left
WBAS [°]
Male
Female
CCW
CW
Left
Right
Down
Up
Away
Towards
Roll velocity [°/s]
Sideslip velocity [m/s]
Lift velocity [m/s]
Thrust velocity [m/s]

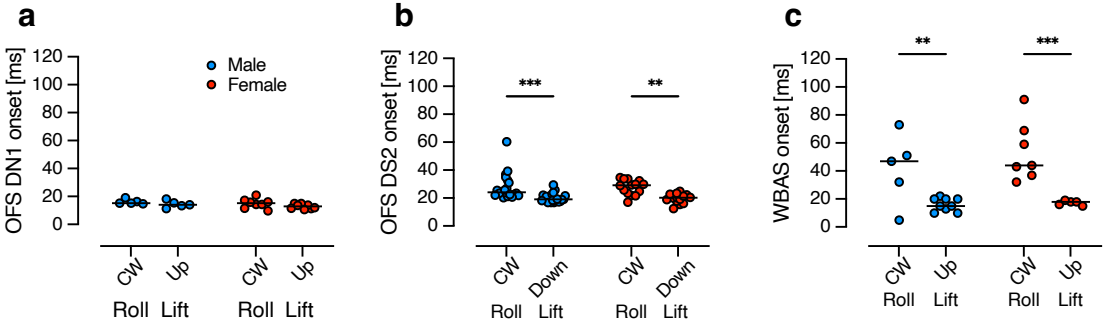
a
OFS DN1 onset [ms]
120
100
80
60
40
20
0
Male
Female
CW
Up
CW
Up
Roll
Lift
Roll
Lift
b
OFS DS2 onset [ms]
120
100
80
60
40
20
0
***
**
CW
Down
CW
Down
Roll
Lift
Roll
Lift
c
WBAS onset [ms]
120
100
80
60
40
20
0
**
***
CW
Up
CW
Up
Roll
Lift
Roll
Lift

Stimulus		Velocity	Sex	Interaction		Velocity	Sex	Interaction
Roll	OFS DN1	****	0.35	0.14	OFS DN2	****	0.31	>0.99
Sideslip		****	0.90	0.12		****	**0.01**	****
Lift		**0.002**	0.86	>0.99		****	0.18	***
Thrust		****	0.11	****		****	0.10	**0.02**
Roll	WBAD	****	0.11	0.66	WBAS	****	0.13	0.76
Sideslip		****	0.76	0.35		****	0.61	0.79
Lift		**0.03**	0.79	0.52		****	0.09	**0.02**
Thrust		0.29	0.66	0.72		***	0.57	0.83

Supplementary information

Sexual dimorphism in sensorimotor transformation of optic flow

Sarah Nicholas[1], Katja Sporar Klinge[1#], Luke Turnbull[1], Annabel Moran[1], Aika Young[1], Yuri Ogawa[1], Karin Nordström[1,2*]*

Supplementary Figure legends

Supplementary Fig 1. Exclusion criteria and receptive field comparisons in male and female OFS DNs. a Distribution of maximum local motion sensitivity (LMS) in 100 male reference neurons (grey histogram, N = 100) compared to the neurons used for quantification in the rest of the paper (N = 35 males, 36 females). Six neurons with a maximum LMS below 20 spikes/s (red cross-hatched region or dashed line) were excluded from further analysis. **b** Number of stimulus positions with LMS greater than 50% of the neuron's maximum LMS (black and red arrows in Fig. 1c and f). Neurons with fewer than 4 positions were excluded. **c** Distribution of LPD variance. Neurons with directional variance exceeding 30° were excluded. **d** Classification of male neurons based on receptive field centre and preferred direction. The top panel shows the preferred directions across neurons, with dashed lines indicating the directional thresholds used for neuron type classification. The middle panel shows receptive field centre locations, and the bottom panel illustrates the relationship between receptive field centre and the receptive field preferred direction for all 35 male neurons, with 2 neurons excluded from further analysis (grey). **e** Same classification criteria applied to 36 female neurons, with 7 neurons excluded (grey). **f** The receptive field width and height at the 50% contour line for the remaining OFS DN 1 (N = 10 males, 12 females) and OFS DN2 (N = 23 males, 17 females). Individual data points shown, with black lines representing the median.

Supplementary Fig 2. Schematic illustration showing the steps used to standardize data across recordings. a. Top panel, ventral-side-up position of hoverfly during electrophysiology recordings. Middle panel, reorientation to display the dorsal visual field at the top. Bottom panel, neurons with receptive fields in the left-hand side (LHS) of the visual field have been mirrored to the right-hand side (RHS). **b** Response of an example neuron to a full-screen, full-contrast sinusoidal grating (spatial wavelength 7°; temporal frequency 5 Hz) moving in eight different directions. The plots illustrate the effect of compensating for hoverfly orientation (middle panel) and receptive field location (bottom panel). The red arrowhead shows the neuron's preferred direction, and the red line indicates response amplitude for full-screen sinusoidal gratings. **c** Preferred direction of male hoverfly OFS DNs (N = 29). Neurons are colour coded by classification, with dashed lines indicating the receptive field thresholds. The plots show the effect of compensating the original data (top) for orientation (middle) and receptive field location (bottom). **d** Preferred direction of female hoverfly OFS DNs (N = 26), as in panel c.

Supplementary Fig. 3. Comparison of spontaneous activity and responses to stationary stimuli. a Spontaneous activity (open shapes) and responses of OFS DN1 to the stationary starfield (filled shapes), from data extracting directional sensitivity (as in Fig. 2; circles) or velocity response functions (as in Fig. 3; triangles). **b** Spontaneous activity and responses of OFS DN2 as in panel a. **c** WBAS before stimulus presentation (open squares) or when viewing the stationary starfield (filled squares), quantified during velocity response function experiments (as in Fig. 5). Individual data points are shown, with lines representing the median. Asterisks denote statistical significance, two-way ANOVA with uncorrected Fisher's LSD test: * $p < 0.05$, ** $p < 0.01$, *** $p < 0.001$ and **** $p < 0.0001$.

Supplementary Fig 4. Morphological quantification of OFS DN2. a Schematic diagram of the hoverfly central brain and thoracic ganglia showing locations where the cervical connective (CC) and the OFS DN2 (orange) widths were measured. **b** Width measurements of OFS DN2 axons along the cervical connective at four anatomical landmarks: (1) immediately posterior to the central brain, (2) upper third of the CC, (3) lower third of the CC, and (4) immediately anterior to the thoracic ganglion. Data are shown for 3 male (blue) and 3 female (red) hoverflies. **c** Width of the anterior end of the cervical connective in the same individuals. All data are presented as individual repeats with the horizontal lines indicating median.

Supplementary Fig 5. Impact of stimulus size on neural and behavioural velocity response functions. a Velocity response functions of male OFS DN2 neurons when the stimulus covered either the full screen (blue) or the central square (black, N = 7). **b** Velocity response functions of WBAS in male hoverflies when the stimulus covered either the full screen (blue) or the central square (black, N = 5). All data are presented as median and interquartile range.

Supplementary Movies

Supplementary Movie 1. Neural response to roll optic flow. The video shows the raw extracellular response of an OFS DN2 in red when the hoverfly was viewing an example roll stimulus, as in Fig. 3 of the main paper.

Supplementary Movie 2. WBA response to sideslip optic flow. The video on the left shows the hoverfly filmed from above, with the coloured dots indicating the points tracked by DeepLabCut to extract the WBA. The stimulus the hoverfly was viewing is displayed on the right, as in Fig. 5 of the main paper.

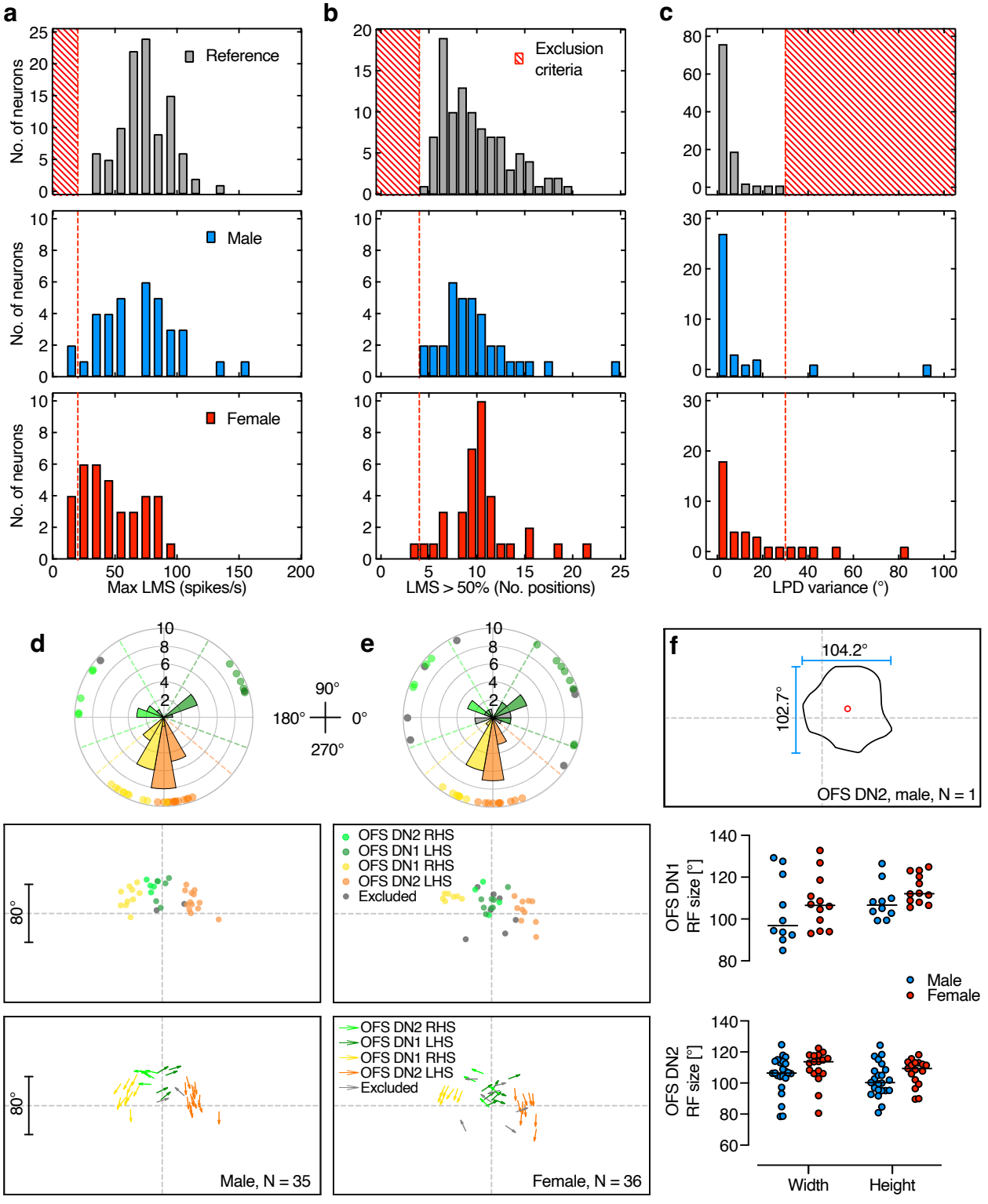
a
b
c
Reference
Exclusion criteria
Male
Female
No. of neurons
Max LMS (spikes/s)
LMS > 50% (No. positions)
LPD variance (°)
d
e
90°
180°
0°
270°
f
104.2°
102.7°
OFS DN2, male, N = 1
OFS DN2 RHS
OFS DN1 LHS
OFS DN1 RHS
OFS DN2 LHS
Excluded
80°
Male, N = 35
Female, N = 36
OFS DN1 RF size [°]
OFS DN2 RF size [°]
Male
Female
Width
Height

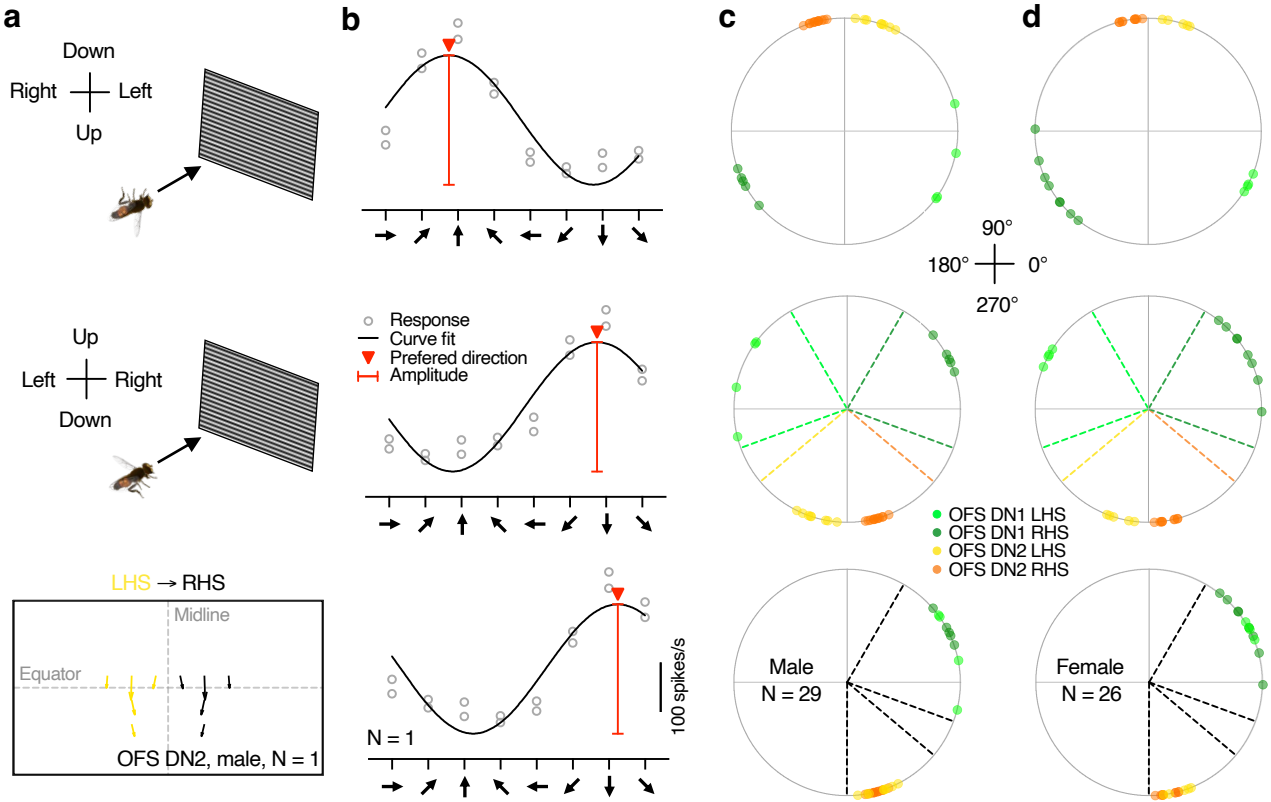
a
Down
Right
Left
Up
Up
Left
Right
Down
LHS → RHS
Midline
Equator
OFS DN2, male, N = 1
b
Response
Curve fit
Prefered direction
Amplitude
N = 1
100 spikes/s
c
d
90°
180°
0°
270°
OFS DN1 LHS
OFS DN1 RHS
OFS DN2 LHS
OFS DN2 RHS
Male
N = 29
Female
N = 26

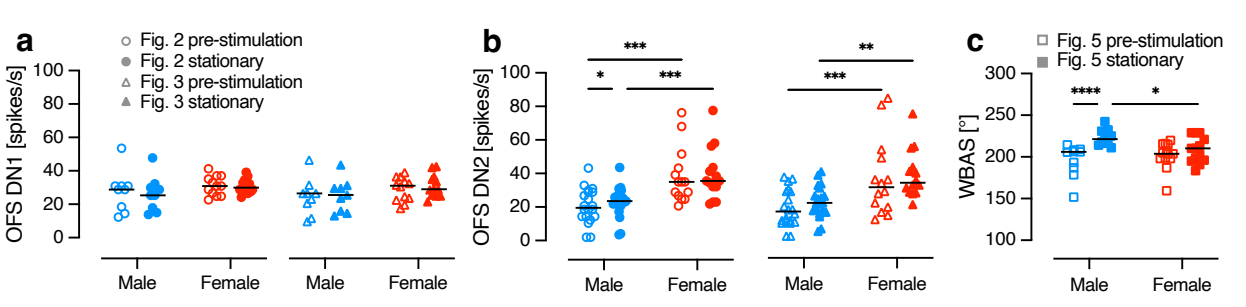
a
Fig. 2 pre-stimulation
Fig. 2 stationary
Fig. 3 pre-stimulation
Fig. 3 stationary
OFS DN1 [spikes/s]
100
80
60
40
20
0
Male
Female
Male
Female
b
OFS DN2 [spikes/s]
100
80
60
40
20
0
***
*
***
**
***
Male
Female
Male
Female
c
Fig. 5 pre-stimulation
Fig. 5 stationary
WBAS [°]
300
250
200
150
100
****
*
Male
Female

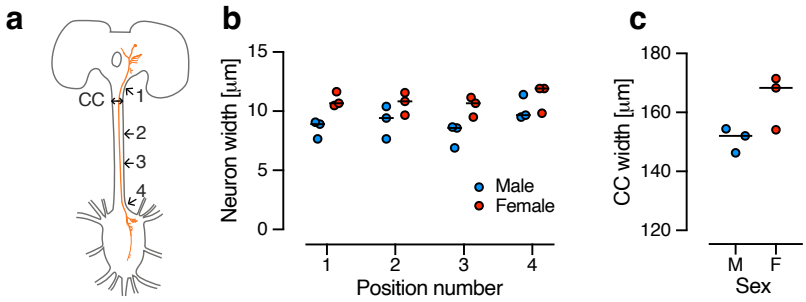
a
CC
0
1
2
3
4
b
Neuron width [µm]
15
10
5
0
1
2
3
4
Position number
Male
Female
c
CC width [µm]
180
160
140
120
M
F
Sex

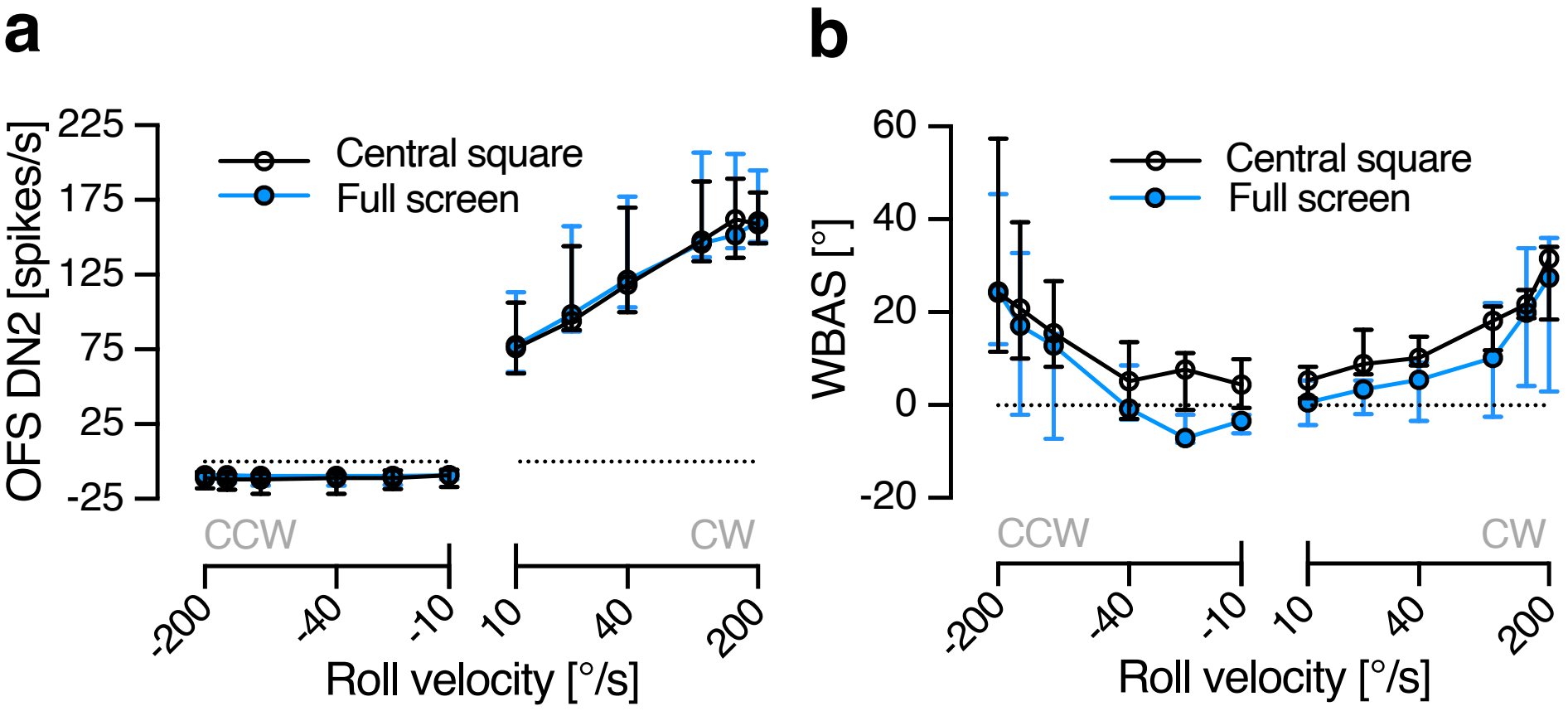
a
b
OFS DN2 [spikes/s]
225
175
125
75
25
-25
Central square
Full screen
CCW
CW
-200
-40
-10
10
40
200
Roll velocity [°/s]
WBAS [°]
60
40
20
0
-20
Central square
Full screen
CCW
CW
-200
-40
-10
10
40
200
Roll velocity [°/s]